Journal of Magnetic Resonance **151,** 32–39 (2001)
doi:10.1006/jmre.2001.2346, available online at http://www.idealibrary.com on IDEAL®

# Analytical Solution to the Lipari–Szabo Model Based on the Reduced Spectral Density Approximation Offers a Novel Protocol for Extracting Motional Parameters

Christian Renner, Luis Moroder, and Tad A. Holak

*Max Planck Institute for Biochemistry, 82152 Martinsried, Germany*

Received October 2, 2000; revised March 30, 2001

**An analytical solution to the Lipari–Szabo model is derived for isotropic overall tumbling. The parameters of the original Lipari–Szabo model, the order parameter $S^2$ and the effective internal correlation time $\tau_e$, are calculated from two values of the spectral density function. If additionally the spectral density value $J(0)$ is known, the exchange contribution $R_{ex}$ term can also be determined. The overall tumbling time $\tau_c$ must be determined in advance, for example, from $T_1/T_2$ ratios. The required spectral density values are obtained by reduced spectral density mapping from $T_1$, $T_2$, and NOE measurements. Our computer simulations show that the reduced spectral density mapping is a very good approximation in almost all cases in which the Lipari–Szabo model is applicable. The robustness of the analytical formula to experimental errors is also investigated by extensive computer simulations and is found to be similar to that of the fitting procedures. The derived formulas were applied to the experimental $^{15}$N relaxation data of ubiquitin. Our results agree well with the published parameter values of $S^2$ and $\tau_e$, which were obtained from standard fitting procedures. The analytical approach to extract parameters of molecular motions may be more robust than standard analyses and provides a safeguard against spurious fitting results, especially for determining the exchange contribution $R_{ex}$.** 

*Key Words:* **high-resolution NMR; $^{15}$N relaxation; spectral density mapping; order parameter; chemical exchange; protein dynamics.**

## INTRODUCTION

One of the strengths of NMR is its ability to study the dynamic behavior of molecules in solution at an atomic level (*1, 2*). Two different approaches currently exist for addressing motions on very different time scales. Motions on slow time scales (seconds to years) are investigated by $^1$H/$^2$D-exchange of exchangeable protons, whereas faster motions (picoseconds to milliseconds) are studied by measurement and evaluation of nuclear spin relaxation rates mainly of $^{15}$N, $^{13}$C, or $^2$H nuclei (*3–5*). Although measurement of $^1$H relaxation is in principle possible, quantitative interpretation is usually hampered by the multitude of relaxation pathways that exist for protons. For the interpretation of the experimental relaxation rates in terms of microscopic parameters of motion a generalized model, often called the "model-free approach," was presented by Lipari and Szabo in 1982 (*6, 7*). In this model motions of a molecule are separated into the overall rotational reorientation and additional internal motions, which are described by one amplitude (order parameter $S^2$) and one time scale (internal effective correlation time $\tau_e$), respectively. The Lipari–Szabo model is not based on a specific physical model (hence the name model-free) and therefore the Lipari–Szabo parameters represent only the simplest generalized description of internal motions. To translate these generalized parameters into specific physical observables a physical model (for example, wobbling in a cone) must be invoked (*8*). The Lipari–Szabo model can be extended to incorporate anisotropy of the overall tumbling of a molecule (*9*). However, Schurr *et al.* (*10*) have shown by computer simulations that for moderate anisotropy ($\sigma < 2.0$) neglecting anisotropy does not affect Lipari–Szabo parameters much. Experimentally, differences between isotropic and anisotropic analysis were also found to be small for moderate anisotropy (*11, 12*). In the original articles Lipari and Szabo presented a simple analytical solution to their model provided internal motions are in the "extreme narrowing" limit (*6*). In the general case fitting procedures are proposed to determine parameter values that optimize agreement between measured relaxation rates and rates calculated from the model. The inability to invert the Lipari–Szabo model has been implied in all applications and has even been stated explicitly (*2, 13*). However, due to its simplicity the Lipari–Szabo model has been very successful for interpretation of $^{15}$N, $^{13}$C, and recently also of $^2$H relaxation rates (*14–19*).

Only more recently was a truly model-free approach, the "full spectral density mapping," developed by Peng and Wagner (*20, 21*). In this approach additional relaxation experiments are introduced to determine the spectral density values at five frequencies. The spectral density at high frequencies was found to be small. Based on this observation 3 years later the "reduced spectral density mapping" method was developed by Farrow *et al.* (*22*) and a similar approach was reported by Ishima and Nagayama (*23*). The methods rely on the approximations of the high frequency values of the spectral density. The reduced



1090-7807/01 $35.00

spectral density mapping approach allows the determination of spectral density values from measured $T_1$, $T_2$, and NOE data alone. The validity of the reduced spectral density mapping approximation was confirmed by full spectral density mapping (*24*). The main application of this approach has been on $^{15}$N relaxation rates of $^{15}$N enriched proteins (*25–27*).

We show in this contribution that when the Lipari–Szabo model is applicable the reduced spectral density approximation works very well over a much larger range of Lipari–Szabo parameter values than those expected so far. The main focus of this study is on an analytical solution of the original isotropic Lipari–Szabo model with two adjustable parameters, $S^2$ and $\tau_e$, and a given overall correlation time $\tau_c$. Formulas are derived that allow calculations of $S^2$ and $\tau_e$ from two (arbitrary) values $J(\omega_1)$ and $J(\omega_2)$ of the spectral density function. The application of these formulas to spectral density values $J(\omega_N)$ and $J(0.87\omega_H)$ obtained by reduced spectral density mapping is proposed for calculating order parameter $S^2$, effective internal correlation times $\tau_e$, and possible exchange contributions $R_{ex}$ from data obtained by standard $^{15}$N relaxation measurements at one field strength, i.e., longitudinal $T_1$, transverse $T_2$, and heteronuclear $^{15}$N{$^1$H} NOE, *without the need of fitting procedures*. Using $J(0)$ allows simple calculation of $S^2$ and $\tau_e$ values. However, measurements at several field strengths are required to determine $J(0)$ values that are not affected by exchange (*28*). We propose to use $J(\omega_N)$ and $J(0.87\omega_H)$ so that exchange broadening and experimental difficulties affecting $T_2$ measurements (as described in Ref. (*29*) and references therein) do not affect the determination of $S^2$ and $\tau_e$. The range of validity and the robustness against experimental errors are tested by extensive computer simulations. Previously published relaxation data for the protein ubiquitin (*11*) are used to compare the results from our analytical formulas with those from common fitting procedures. Although we focus mainly on $^{15}$N relaxation of proteins, the approach derived herein is applicable whenever at least two values of the spectral density function can be determined.

## THEORY

*The Lipari–Szabo model.* The experimentally accessible relaxation rates $T_1$, $T_2$, and NOE are functions of the spectral density $J(\omega)$ at various frequencies $\omega$ (*30*). As the formulas for $T_1$, $T_2$, and NOE contain five spectral density values, a direct inversion of the equations is not possible. In the Lipari–Szabo approach a model function for $J(\omega)$ with only two adjustable parameter $S^2$ and $\tau_e$ is assumed (*6*):

$$J(\omega) = \frac{2}{5}\left(\frac{S^2\tau_c}{1+\omega^2\tau_c^2} + \frac{(1-S^2)\tau_e}{1+\omega^2\tau_e^2}\right). \qquad [1]$$

The effective internal correlation time $\tau_e$ is connected to the internal correlation time $\tau_i$ by $1/\tau_e = 1/\tau_i + 1/\tau_c$. The overall correlation time $\tau_c$ is the same for the whole molecule and is usually determined from $T_1/T_2$ ratios (*11*, *14*). In the extreme narrowing limit, i.e., when $\omega^2\tau_e^2 \ll 1$, the second term of the Lipari–Szabo model function can be approximated by $(1-S^2)\tau_e$ (*6*). In this case, analytical expressions for $S^2$ and $\tau_e$ are obtained immediately:

$$S^2 = \frac{5}{2}(J(\omega_1) - J(\omega_2))\left(\frac{\tau_c}{1+\omega_1^2\tau_c^2} - \frac{\tau_c}{1+\omega_2^2\tau_c^2}\right)^{-1}. \qquad [2]$$

Computer simulations, as described below, indicate that using $\omega_1 = 0.87\,\omega_H$ and $\omega_2 = \omega_N$ (reduced spectral density mapping) this approximation gives good results for $0.87\omega_H\,\tau_e < 0.6$, e.g., for $\tau_i < 200$ ps at 600 MHz proton frequency (unpublished results). For $\tau_i > 200$ ps the approximation (Eq. [2]) is no longer valid.

*Reduced spectral density mapping.* The spectral density function $J(\omega)$ has small values for $\omega = \omega_H$ ($^1$H angular spin precession frequency) as shown by Peng and Wagner (*20*, *21*) and Lefèvre *et al.* (*24*). Therefore, it can be assumed that it varies only little in the vicinity of $\omega_H$. In the reduced spectral density approach the spectral density values $J(0)$, $J(\omega_N)$, and $J(0.87\omega_H)$ are calculated from the $^{15}$N $T_1$, $T_2$, and NOE using the approximation $J(\omega) \propto 1/\omega^2$ for $\omega = \omega_H \pm \omega_N$ (*22*):

$$\begin{aligned} J(0.87\omega_H) &= \left(\frac{4}{5d^2}\right)\left(\frac{\gamma_N}{\gamma_H}\right)\frac{(\mathrm{NOE}-1)}{T_1} \\ J(\omega_N) &= \frac{1}{T_1}\left(1 - \frac{7}{5}\frac{\gamma_N}{\gamma_H}(\mathrm{NOE}-1)\right)\Big/\left(\frac{3d^2}{4} + c^2\right) \\ J(0) &= \left(\frac{1}{T_2} - \frac{1}{T_1}\left(\frac{1}{2} + \frac{3}{5}\frac{\gamma_N}{\gamma_H}(\mathrm{NOE}-1)\right)\right)\Big/ \\ &\quad \times\left(\frac{d^2}{2} + \frac{2c^2}{3}\right), \end{aligned} \qquad [3]$$

with $c$ and $d$ as in Farrow *et al.* (*22*): $c^2 = \omega_N^2(\sigma_| - \sigma_\perp)^2/3$, $d = (\mu_0\gamma_H\gamma_N h/(8\pi^2))/ < 1/r_{NH}{}^3 > (d^2/4 \approx 1.3\,10^9\,\mathrm{s}^{-2}$, $c^2 \approx 0.9\,10^9\,\mathrm{s}^{-2}$ at 500 MHz proton frequency) where symbols have their usual meanings.

*Derivation of the analytical solution.* $\omega_1$ and $\omega_2$ are defined as two frequencies for which the spectral density $J(\omega)$ is known. $S^2$, $\tau_c$, $\tau_e$, and $R_{ex}$ are Lipari–Szabo parameters as before. Defining $C(\omega) = 2.5\,J(\omega)(1+\omega^2\tau_c^2)$ we obtain for the Lipari–Szabo model

$$C(\omega_i)\left(1+\omega_i^2\tau_e^2\right) = \left[S^2\tau_c\left(1+\omega_i^2\tau_e^2\right) + (1-S^2)\tau_e\left(1+\omega_i^2\tau_c^2\right)\right]. \qquad [4]$$

Setting $\omega_i = \omega_1$ and adding on the left side

$$S^2\omega_2^2\tau_c\tau_e^2 + (1-S^2)\omega_2^2\tau_c^2\tau_e - S^2\omega_2^2\tau_c\tau_e^2 - (1-S^2)\omega_2^2\tau_c^2\tau_e = 0, \qquad [5]$$

one obtains after rearrangement of the terms and application of Eq. [4] with $\omega_i = \omega_2$

$$C(\omega_1)\left(1+\omega_1^2\tau_e^2\right) = C(\omega_2)\left(1+\omega_2^2\tau_e^2\right) + \tau_c\tau_e\left(\omega_1^2-\omega_2^2\right)[S^2(\tau_e-\tau_c)+\tau_c]. \quad [6]$$

Equation [4] with $\omega_i = \omega_2$ is solved for $S^2(\tau_e - \tau_c)$ and inserted in Eq. [6]. After some algebra one obtains

$$C(\omega_1)\left(1+\omega_1^2\tau_e^2\right) = C(\omega_2)\left(1+\omega_2^2\tau_e^2\right)\left[1+\frac{\tau_c\tau_e\left(\omega_1^2-\omega_2^2\right)}{\omega_2^2\tau_c\tau_e-1}\right] - \frac{\tau_c\tau_e\left(\omega_1^2-\omega_2^2\right)(\tau_e+\tau_c)}{\omega_2^2\tau_c\tau_e-1}. \quad [7]$$

Multiplication with $\omega_2^2\tau_c\tau_e - 1$ yields an equation of third order in $\tau_e$,

$$\begin{aligned}&\tau_e^3[C(\omega_1)-C(\omega_2)]\omega_1^2\omega_2^2\tau_c + \tau_e^2\left[C(\omega_2)\omega_2^2 - C(\omega_1)\omega_1^2\right.\\ &\left.+\tau_c\left(\omega_1^2-\omega_2^2\right)\right] + \tau_e\left[C(\omega_1)\omega_2^2\tau_c - C(\omega_2)\omega_1^2\tau_c\right.\\ &\left.+\tau_c^2\left(\omega_1^2-\omega_2^2\right)\right] + C(\omega_2) - C(\omega_1) = 0. \quad [8]\end{aligned}$$

$J(0.87\omega_H)$ and $J(\omega_N)$ can be calculated with the reduced spectral density approach from $T_1$ and heteronuclear NOE. For $\omega_1$ and $\omega_2$ one inserts 0.87 $\omega_H$ and $\omega_N$ and obtains $\tau_e$ as the solution of Eq. [8] that lies between zero and $\tau_c$. It is important to note that Eq. [8] is valid for all $\tau_e$ if the dependence of $C(\omega_i)$ on $\tau_e$ is taken into account. In our approach we determine $C(\omega_i)$ from experimental relaxation rates and consider them constant in the search for a $\tau_e$ that fulfils Eq. [8]. Only with constant $C(\omega_i)$ does Eq. [8] represent a third-order equation for $\tau_e$. A general proof of the existence of a unique solution is hampered by the fact that the $C(\omega_i)$ have few general properties that can be exploited for such a proof. However, we have investigated this problem with computer simulations covering all possible Lipari–Szabo parameter combinations and have obtained in all cases a unique solution, thus providing empirical evidence that always exactly one solution to Eq. [8] is found (for details see the Supporting Information).

Using again Eq. [4], $S^2$ can be calculated as

$$S^2 = \frac{\left[C(\omega_2)\left(1+\omega_2^2\tau_e^2\right) - \tau_e\left(1+\omega_2^2\tau_c^2\right)\right]}{(\tau_e-\tau_c)\left(\omega_2^2\tau_c\tau_e-1\right)}. \quad [9]$$

$J(0)$ calculated with the reduced spectral density mapping (Eq. [3]) depends on $T_2$ and therefore contains the exchange contribution $R_{ex}$,

$$R_{ex} = \left[J(0) - \frac{2}{5}(S^2\tau_c + \tau_e - S^2\tau_e)\right](d^2/2 + 2c^2/3). \quad [10]$$

It has been assumed several times in the derivation of the above equations that $\omega_2^2\tau_c\tau_e - 1 \neq 0$. This is no restriction on $\omega_2$ as the derivation and final solution are completely symmetrical with respect to $\omega_1$ and $\omega_2$. Therefore, $\omega_2$ can always be chosen appropriately ($\omega_N$ or $0.87\omega_H$), so that $\omega_2^2\tau_c\tau_e - 1 \neq 0$ is fulfilled. Usually $J(\omega_N)$ is known to higher precision than $J(0.87\omega_H)$ so that it is recommendable to use $\omega_2 = \omega_N$, if possible.

In the presence of moderate anisotropy order parameters $S^2$ and internal correlation times $\tau_i$ remain largely unaffected (*10*, *11*), thus justifying the application of Eqs. [8]–[10]. The exchange contribution $R_{ex}$, however, is dependent on anisotropy of the overall tumbling (*11*, *27*). Therefore, Eq. [10] must be replaced by

$$R_{ex} = \left\{J(0) - \frac{2}{5}\left[S^2\sum_{n=1}^{5}A_n\tau_n + (1-S^2)\tau_e\right]\right\} \times (d^2/2 + 2c^2/3), \quad [11]$$

with the $A_n$ and $\tau_n$ defined by the fully asymmetric diffusion tensor (*11*). $\tau_e$ is in this case calculated as $1/\tau_e = 5/\tau_1 + 5/\tau_2 + 5/\tau_3 + 5/\tau_4 + 5/\tau_5 + 5/\tau_i$.

## COMPUTER SIMULATIONS

Synthetic $T_1$, $T_2$, and NOE data were generated randomly at proton frequencies of 500 and 600 MHz for 10,000 virtual $^{15}N$ nuclei (assuming one attached proton as in the protein backbone). From homogeneously distributed random numbers $X(1), X(2), X(3) \in [0, 1]$, ($P(X) =$ const.) order parameters $S^2$, internal correlation times $\tau_i$, and exchange contributions $R_{ex}$ were calculated as follows: $S^2 = 0.9–0.8 * X(1)^2$, $\tau_i = 0.7 * X(2) * 10^{4X(2)}$ ps, $R_{ex} = X(3)^2 * 10$ Hz. The effective internal correlation time $\tau_e$ is given by $1/\tau_e = 1/\tau_i + 1/\tau_c$. The isotropic Lipari-Szabo model with a constant overall correlation time $\tau_c$ of 7.0 ns was used to generate $T_1$, $T_2$, and NOE values. From the spectral densities obtained by Eq. [1] $T_1$, $T_2$, and NOE at magnetic field strengths of 500 and 600 MHz proton frequency were calculated with the well-known formulas (*14–17*). Parameter combinations that resulted in $T_1$ times longer than 5 s were discarded (9 cases of 10,000). For the test of the analytical solution Gaussian noise with a standard deviation of 1, 3, and 5% was added to the relaxation rates resulting in three different data sets, each comprising $T_1$, $T_2$, and NOE values at two field strengths for 9991 virtual nuclei.

Testing of the reduced spectral density mapping approximation $J(\omega) \propto 1/\omega^2$ for $\omega = \omega_H \pm \omega_N$, as proposed by Farrow *et al.* (*22*), was performed using a noise-free data set. $J(0)$ was not calculated according to Eq. [3], but using Eqs. [19] and [20] of Farrow *et al.* (*22*) because exchange contributions $R_{ex}$ were present in our synthetic $T_2$ values.

Tests of the analytical solution were performed on the data sets containing 1, 3, or 5% Gaussian errors. $J(0)$, $J(\omega_N)$, and $J(0.87\omega_H)$ were calculated with Eq. [3] from $T_1$, $T_2$, and NOE

at one field strength. The overall correlation time $\tau_c$ was set to 6.5 (too short), 7.0 (correct), and 7.5 ns (too long) in different calculations to investigate the influence of error in the $\tau_c$ value on the resulting Lipari–Szabo parameters. From $J(\omega_N)$ and $J(0.87\omega_H)$ the effective internal correlation time $\tau_e$ was determined as the solution of Eq. [8] that lies between 0 and $\tau_c$. If no solution was found in this range, we decreased the lower limit from zero to $-10$ ps because statistical errors can shift the solution of Eq. [8] to small negative values. In all the simulations for every $T_1$, $T_2$, NOE triple a solution to Eq. [8] could be found between $-10$ ps and $\tau_c$. The order parameter $S^2$ was calculated using Eq. [9], and the exchange contribution $R_{ex}$ was then determined from $J(0)$, $S^2$, and $\tau_e$ using Eq. [10]. It should be emphasized that the appearance of negative times is only due to errors present in the $T_1$ and NOE values and negative $\tau_e$ should be replaced by zero (after calculation of $S^2$ and $R_{ex}$).

We found for all three simulated cases that NOE values higher than the theoretical maximum lead to strong overestimation of $\tau_e$ and subsequently often to $S^2$ values $>1$ or $<0$. Therefore, we used the theoretical maximum for the NOE in all our calculations whenever the NOE value (caused by experimental error) was higher than the field-dependent maximum.

## RESULTS

Unless stated otherwise, all calculations were performed using the $^{15}$N $T_1$, $T_2$, and hetNOE values calculated for a proton frequency of 600 MHz. Figure 1 shows good agreement between spectral densities values obtained from $^{15}$N $T_1$, $T_2$, and hetNOE using the reduced spectral density approximation and the true spectral densities that were used to generate the $^{15}$N $T_1$, $T_2$, and hetNOE data. Even in cases of high mobility, as indicated by large $J(0.87\omega_H)$ and small $J(0)$ values, almost no visible deviations from the straight line $y = x$ can be seen. The relative deviation of the back-calculated spectral densities from the original ones averaged over the whole data set of 9991 virtual residues is given in the first column of Table 1. Excluding

**TABLE 1**

**Relative rmsd between Spectral Densities Calculated with the Reduced Spectral Density Mapping Approximation and True Values ($=100\% * (J_{approx}/J_{true} - 1)$) Averaged over Subsets of the Whole Data Set Comprising 9991 Virtual Residues**

| Rel. rmsd | All[a] | $S^2 > 0.5$[b] | $S^2 > 0.7$[c] | Max.[d] |
|---|---|---|---|---|
| $J(0)$ | 0.50% | 0.11% | 0.05% | 5.6% |
| $J(\omega_N)$ | 0.83% | 0.24% | 0.13% | 7.2% |
| $J(0.87\omega_H)$ | 0.19% | 0.17% | 0.15% | 0.8% |

[a] See Computer Simulation for the generation of the data set of 9991 virtual residues.

[b] Data generated with $S^2 < 0.5$ are excluded from averaging.

[c] Data generated with $S^2 < 0.7$ are excluded.

[d] For all spectral densities the maximum deviation occurs for $\tau_e \approx 1/\omega_H$, $S^2 \approx 0.1$ (no $S^2 < 0.1$ are included).

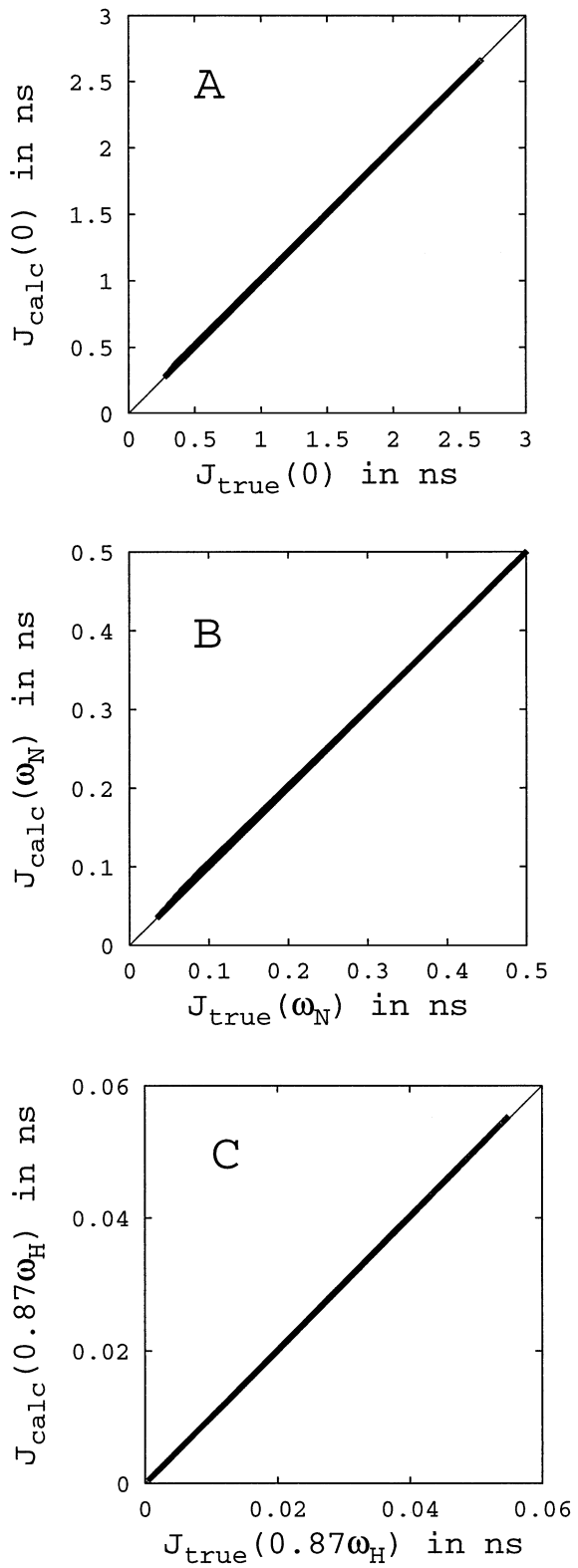


**FIG. 1.** Correlation between spectral densities values obtained from $^{15}$N $T_1$, $T_2$, and hetNOE using the reduced spectral density approximation and the true spectral densities that were used to generate the $^{15}$N $T_1$, $T_2$, and hetNOE data. A, B, and C show the results for $J(0)$, $J(\omega_N)$, and $J(0.87 * \omega_H)$, respectively.

residues with small $S^2$ reduces the rmsd relative to the rmsd for all residues (Table 1). This reflects the well-known fact that the reduced spectral density mapping works best for rigid residues (*22*). The largest deviations are present for $\tau_e \approx 1/\omega_H$ and these decrease with increasing $S^2$. The derivative of the maximum deviation with respect to $S^2$ is largest for small $S^2$ in the case of $J(0)$ and $J(\omega_N)$, whereas for $J(0.87\omega_H)$ the opposite is true.

The robustness of our analytical solution in the presence of random errors in the relaxation rates was tested also for the data set of 9991 virtual residues modified by addition of 1, 3, or 5% Gaussian errors to the $T_1$, $T_2$, and hetNOE values (calculated at 600 MHz proton frequency). In additional calculations the overall correlation time $\tau_c$ was deliberately offset by 0.5 ns from the value that was used in the generation of the synthetic relaxation rates (too short: $\tau_c = 6.5$ ns, too long: $\tau_c = 7.5$ ns). For all cases, $S^2$, $\tau_e$, and $R_{ex}$ were also obtained by fitting the isotropic Lipari–Szabo model with exchange contributions to the relaxation rates using the same $\tau_c$ as above (i.e., the parameters used were $S^2$, $\tau_e$, $R_{ex}$). Figures 2A and 2B show the correlation between original and back-calculated $\tau_e$ values for $\tau_c = 7.0$ ns and 3% Gaussian noise using the analytical solution and the common procedure of model fitting, respectively. Both figures include also the results that are obtained when using an error-free data set, thus proving the correctness of both methods. Obviously, fitting leads to an underestimation of the $\tau_e$ values in some cases; this is not observed for the analytical solutions.

The accuracy and precision of $S^2$ and $R_{ex}$ were assessed by calculating the mean value and standard deviation of the difference between the back-calculated and original parameter values. The comparison of the analytical solution with the fitting procedure is summarized in Table 2. The very few cases where the analytical solution did not result in meaningful results for $S^2$(>1 or <0) were not included in the mean value or standard deviation, but the number of such occurrences is reported in Table 2. On the other hand, the exchange contribution $R_{ex}$ and the effective internal correlation time $\tau_e$ were not restricted to positive values. A table comparing analytical solution and fitting procedure using $\tau_c = 6.5$ ns and $\tau_c = 7.5$ ns can be found in the Supporting Information. For both methods overestimating $\tau_c$ by 0.5 ns (=7%) leads to $R_{ex}$ values that are on average ≈0.6 Hz too small, whereas $\tau_c = 6.5$ ns results in $R_{ex}$ exceeding the true values on average by ≈0.6 Hz. Surprisingly, this is still true if one uses data at two field strengths (proton frequency of 500 and 600 MHz) simultaneously for the fitting procedure (see Supporting Information). The analytical solution does not benefit as much from additional data as the fitting procedures, as it is not possible to use all of the data simultaneously. Instead,

**TABLE 2**

**Mean Values and Standard Deviations of the Difference between the Back-Calculated and Original $S^2$ and $R_{ex}$ Values Comparing Accuracy and Precision of the Analytical Solution with the Fitting Procedure**

| Amount of error in the data (%) | No. ($S^2 > 1$ or $S^2 < 0$)[a] | Analytical solution, $S^2$(calc)-$S^2$(true) | | Fitting procedure, $S^2$(fit)-$S^2$(true) | |
|---|---|---|---|---|---|
| | | Mean | S.D.[b] | Mean | S.D.[b] |
| 1 | 1 | 0.0002 | 0.014 | 0.0007 | 0.012 |
| 3 | 6 | −0.002 | 0.036 | 0.005 | 0.042 |
| 5 | 55 | −0.005 | 0.056 | 0.011 | 0.07 |
| | | $R_{ex}$(calc)-$R_{ex}$(true) | | $R_{ex}$(fit)-$R_{ex}$(true) | |
| 1 | 1 | −0.002 | 0.15 | −0.006 | 0.14 |
| 3 | 6 | 0.017 | 0.44 | −0.041 | 0.42 |
| 5 | 55 | 0.058 | 0.72 | −0.097 | 0.7 |

[a] Number of cases of the total of 9991 resulting in $S^2 > 1$ or $S^2 < 0$ for the analytical solution.

[b] Standard deviation.

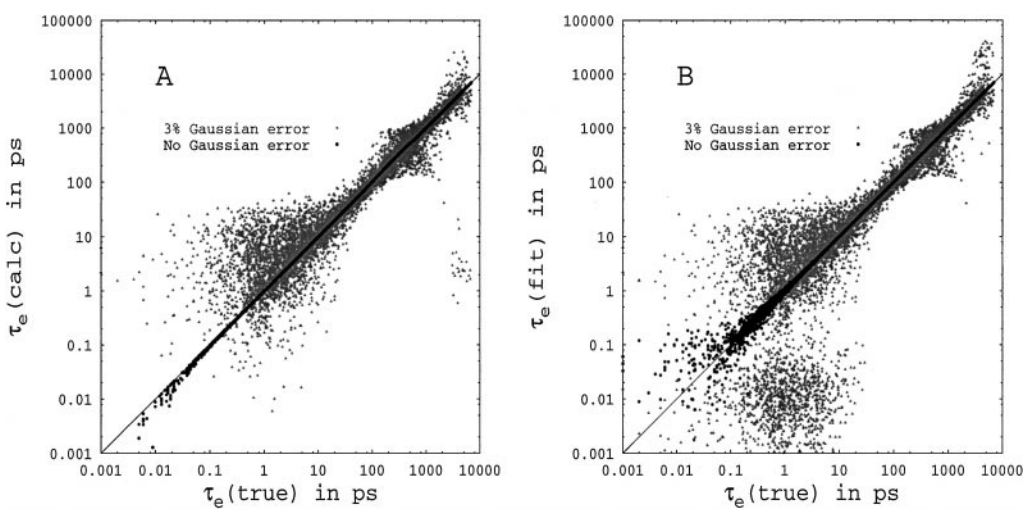


**FIG. 2.** Correlation between original and back-calculated $\tau_e$ values for $\tau_c = 7.0$ ns and 3% Gaussian noise (gray symbols). A and B show the results for the analytical solution and the common procedure of model fitting, respectively. The black symbols represent the results that were obtained from an error-free data set (ideally they should all lie on the diagonal $y = x$). Deviations are observed only for very small $\tau_e$ values (<1ps).

independent parameter sets of $S^2$, $\tau_e$, and $R_{ex}$ can be calculated and averaged. If data from several field strengths are available many different combinations of spectral density values can be used. $S^2$ and $\tau_e$ can be calculated from any $J(\omega_1)$, $J(\omega_2)$ pairs using Eqs. [8] and [9] provided that $\omega_{1/2} > 0$ (that is, no exchange contribution is present in $J(\omega_{1/2})$). $R_{ex}$ is then given by Eq. [10] using any of the $J(0)$ values. Of course, not all possible combinations are independent.

To test our analytical solution on experimental data, we used relaxation rates for ubiquitin published by Tjandra *et al.* (*11*). Ubiquitin is a small and well-characterized protein of 76 residues. It was chosen for its small amount of anisotropy in the overall rotational diffusion (anisotropy factor $\sigma = 1.17$) and for the high quality of the experimental data (obtained at a field strength of 600 MHz). After $S^2$, $\tau_e$, and $R_{ex}$ were calculated negative values for $\tau_e$ and $R_{ex}$ were replaced by zeros (as these parameters are restricted to positive values in the fitting procedure also). The few negative excursions were all small ($\tau_e > -23$ ps, $R_{ex} > -0.6$ Hz in all cases). Four C-terminal residues (73–76) were excluded from the comparison, because the $S^2$, $\tau_e$, $R_{ex}$ Lipari–Szabo model could not reproduce the measured relaxation rates satisfactorily indicating that the Lipari–Szabo model is not adequate for the description of the dynamic behavior of these residues. It has been observed in many studies that the simple Lipari–Szabo model was not applicable to some terminal residues (*15*, *16*, *26*, *31*). More complicated models, usually with two internal time scales, can be invoked for those residues (*15*, *32*). Figure 3 shows the agreement between published $S^2$ and $\tau_e$ parameters for the isotropic $S^2$, $\tau_e$ model and the results obtained with our analytical solution. In both cases $\tau_c = 4.09$ ns was used. The pairwise rmsd is $< 0.02$ for $S^2$ and 3.5 ps for $\tau_e$. Tjandra *et al.* (*11*) have excluded residues 18, 23, 25, and 36 from their analysis as having a significant conformational exchange contribution to the transverse relaxation rate. Exactly these residues have $R_{ex}$ values larger than 0.5 Hz in our calculations. Using the $S^2$, $\tau_e$, $R_{ex}$ model instead of the $S^2$, $\tau_e$ model in the fitting procedure reduces the rmsd between fitting procedure and analytical solution to 0.01 for $S^2$ and 2 ps for $\tau_e$. The rmsd for $R_{ex}$ is 0.002 Hz in this case. All results for the relaxation data of ubiquitin are listed in detail in the Supporting Information.

## DISCUSSION

Applicability of the reduced spectral density mapping has been so far assumed to be limited to cases of low mobility (*22*, *24*). Our simulations show that even in the presence of high flexibility (order parameters $S^2$ as low as 0.1) the reduced spectral density approximation works well. Therefore, we have combined the reduced spectral density mapping with analytical formulas that calculate $S^2$ and $\tau_e$ from the spectral density at two frequencies. Possible exchange contributions are derived subsequently and do not influence the determination of $S^2$ and $\tau_e$. This is in contrast to fitting procedures for which a decision has to be made in advance whether to include $R_{ex}$ or not. In our simulations we found that the analytical solution is more accurate than the fitting procedure using data from one field strength and slightly more precise in the $S^2$ values. Precision of the $R_{ex}$ is the same for both methods. Inaccuracy in the overall tumbling time $\tau_c$ affects both methods in the same way. Although the differences are too small to claim superiority of our new approach for extracting parameters of motion from the relaxation rates, it is at least clear that both methods, the analytical

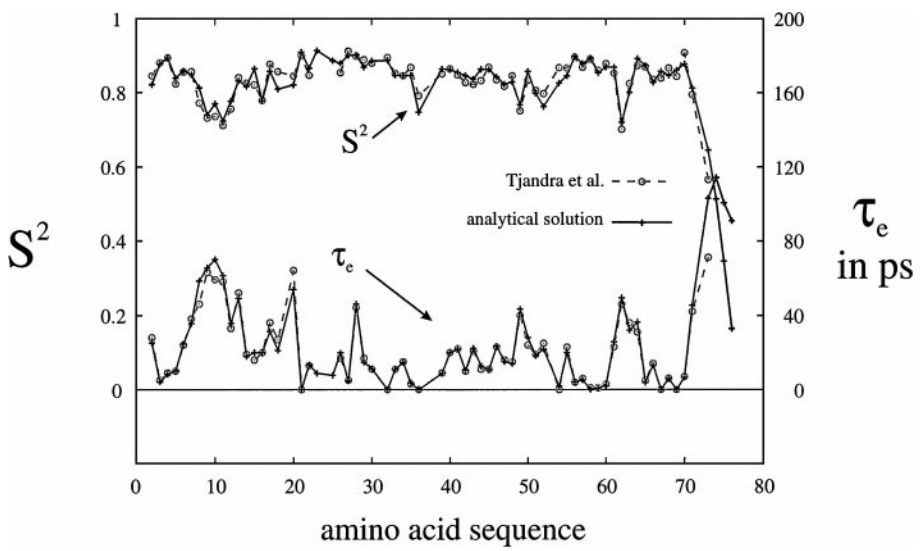


**FIG. 3.** Lipari–Szabo parameters $S^2$ and $\tau_e$ extracted from the published $^{15}$N NMR relaxation measurements on ubiquitin (*11*). Circles connected by broken lines represent published parameter values obtained by fitting to the experimental rates with $\tau_c = 4.09$ ns whereas crosses connected by full lines show the results of our analytical solution again with $\tau_c = 4.09$ ns.

solution and the fitting procedure, perform almost equally well in the interpretation of relaxation data in terms of Lipari–Szabo parameters in the isotropic case. The advantage of the analytical solution is that the motional parameters can be calculated straightforwardly without the need for fitting routines. This can save quite some time when computing errors in the Lipari–Szabo parameters by the common Monte-Carlo method. With fitting procedures and hundred Monte-Carlo rounds per residue our SGI-O2 workstations need some minutes of time per residue, resulting in several hours for a medium-sized protein whereas the analytical approach does not need any appreciable time for computation. Also, it represents a completely new method for obtaining Lipari–Szabo parameters. A current drawback is that Eqs. [8]–[10] are only valid for isotropic overall tumbling. Since the first application of an anisotropic Lipari–Szabo model to protein $^{15}$N relaxation rates (*33*), it has been shown many times that anisotropic tumbling can be detected from the $^{15}$N relaxation rates. For our test case, ubiquitin, an anisotropy factor as small as $\sigma = 1.17$ could be determined with statistical significance due to the very high quality of the experimental data. However, the rmsd between Lipari–Szabo parameters from the isotropic and the anisotropic analysis are as small as 0.005 for $S^2$ and 1.5 ps for $\tau_i$ (*11*). Statistical errors in these parameters are usually much larger. This is in agreement with the theoretical study of Schurr *et al.* (*10*) where it was found that moderate anisotropy ($\sigma < 2.0$) does not affect Lipari–Szabo parameters much, as well as with our own experience (*12*). The only parameter that seems to exhibit some sensitivity toward anisotropy is the exchange contribution $R_{ex}$ (*11*, *27*). With our analytical approach we calculate $S^2$ and $\tau_i$ with Eqs. [8] and [9] assuming isotropic tumbling. For the subsequent calculation of $R_{ex}$ anisotropy can be taken into account using Eq. [11].

Several modifications of the method can be derived using different pairs of spectral density values in Eqs. [8]–[10]. For $^{15}$N relaxation the following simplification is possible (if exchange broadening can be ruled out by additional experiments): the two frequencies used in the analytical solution can be set to zero and $\omega_N$ and in cases of low mobility $S^2$ and $\tau_e$ can be calculated from $T_1$ and $T_2$ alone. The contribution of (NOE-1) to $J(\omega_N)$ in Eq. [3] is scaled down by $\gamma_N/\gamma_H \approx 0.1$. Therefore, the theoretical maximum for the NOEs can be used in Eq. [3] instead of the real value, if the real NOE does not deviate too much from the maximum. As the NOE experiment is less sensitive than $T_1$ or $T_2$ experiments, this simplification can save substantial measurement time (when applicable). Although not shown explicitly in this paper, the analytical solution is not limited to $^{15}$N relaxation, but can be applied whenever the spectral density can be evaluated at two different frequencies.

## CONCLUSIONS

From our results it can be concluded that our analytical solution combined with the reduced spectral density mapping works equally well compared to fitting procedures in determining microscopic parameters of motion ($S^2$, $\tau_e$, $R_{ex}$). In very few cases (0.6% for the data set with 5% Gaussian error) no meaningful results for $S^2$ were obtained in the simulations ($S^2 > 1$ or $S^2 < 0$). The application of our analytical solution to experimental $^{15}$N relaxation data for ubiquitin leads to Lipari–Szabo parameters that are in very good agreement with published values derived from the same experimental relaxation rates.

*Supporting information.* The Supporting Information contains details of the computer simulations providing empirical evidence that always exactly one solution to Eq. [8] is found between zero and $\tau_c$ ( 3 pages) plus four tables (6 pages): three tables compare the analytical solution and fitting procedure using (a) too low (6.5 ns) values for $\tau_c$, (b) too high (7.5 ns) values for $\tau_c$, and (c) data from two field strengths simultaneously. The fourth table compares the Lipari–Szabo parameters obtained by different calculations from the published experimental relaxation rates for the protein ubiquitin. This material is available from the authors.

## ACKNOWLEDGMENT

This work was supported by the Deutsche Forschungsgemeinschaft (SFB 533).

## REFERENCES

1. A. G. Palmer, Probing molecular motion by NMR, *Curr. Opin. Struct. Biol.* **7,** 732–737 (1997).
2. M. W. F. Fischer, A. Majumdar, and E. R. P. Zuiderweg, Protein NMR relaxation: Theory, applications and outlook. *Prog. NMR Spectrosc*. **33,** 207–272 (1998).
3. K. T. Dayie, G. Wagner, and J.-F. Lefèvre, Heteronuclear relaxation and the experimental determination of the spectral density function, *in* "Dynamics and the Problem of Recognition in Biological Macromolecules" (O. Jardetzky and J.-F. Lefèvre, Eds.), NATO ASI Series A, Vol. 288, Plenum Press, New York, 1996.
4. L. E. Kay, Protein Dynamics from NMR. *Biochem. Cell Biol.* **76,** 145–152 (1998).
5. J. P. Loria, M. Rance, and A. G. Palmer, A relaxation-compensated Carr–Purcell–Meiboom–Gill sequence for characterizing chemical exchange by NMR spectroscopy, *J. Am. Chem. Soc*. **121,** 2331–2332 (1999).
6. G. Lipari and A. Szabo, Model-free approach to the interpretation of nuclear magnetic resonance relaxation in macromolecules. 1. Theory and range of validity. *J. Am. Chem. Soc*. **104,** 4546–4559 (1982).
7. G. Lipari and A. Szabo, Model-free approach to the interpretation of nuclear magnetic resonance relaxation in macromolecules. 2. Analysis of experimental results. *J. Am. Chem. Soc.* **104,** 4559–4570 (1982).
8. Z. Zheng, J. Czaplicki, and O. Jardetzky, Backbone dynamics of *trp* repressor studied by $^{15}$N NMR relaxation. *Biochemistry* **34,** 5212–5223 (1995).
9. D. E. Woessner, Nuclear spin relaxation in ellipsoids undergoing rotational Brownian motion. *J. Chem. Phys.* **37,** 647–654 (1962).
10. J. M. Schurr, H. P. Babcock, and B. S. Fujimoto, A test of the model-free formulas. Effects of anisotropic rotational diffusion and dimerization. *J. Magn. Reson. B* **105,** 211–224 (1994).
11. N. Tjandra, S. E. Feller, R. W. Pastor, and A. Bax, Rotational diffusion anisotropy of human ubiquitin from $^{15}$N NMR relaxation. *J. Am. Chem. Soc*. **117,** 12562–12566 (1995).

12. C. Renner and T. A. Holak, NMR $^{15}$N relaxation of the IGF-binding domain of the insulin-like growth factor binding protein 5 (IGFBP-5) determined free in solution and in complex with IGF-II. *Eur. J. Biochem.* **268,** 1058–1065 (2001).
13. D. Jin, M. Andrec, G. T. Montelione, and R. M. Levy, Propagation of experimental uncertainties using the Lipari–Szabo model-free analysis of protein dynamics *J. Biomol. NMR* **12,** 471–492 (1998).
14. L. E. Kay, D. A. Torchia, and A. Bax, Backbone dynamics of proteins as studied by $^{15}$N inverse detected heteronuclear NMR spectroscopy: Application to staphylococcal nuclease. *Biochemistry* **28,** 8972–8979 (1989).
15. G. M. Clore, P. C. Driscoll, P. T. Wingfield, and A. M. Gronenborn, Analysis of the backbone dynamics of interleukin-1$\beta$ using two-dimensional inverse detected heteronuclear $^{15}$N–$^{1}$H NMR spectroscopy. *Biochemistry* **27,** 7387–7401 (1990).
16. N. A. Farrow, R. Muhandiram, A. U. Singer, S. M. Pascal, C. M. Kay, G. Gish, S. E. Shoelson, T. Pawson, J. D. Foreman-Kay, and L. E. Kay, Backbone dynamics of a free and a phosphopeptide-complexed Src homology 2 domain studied by $^{15}$N NMR relaxation. *Biochemistry* **33,** 5984–6003 (1994).
17. T. Zink, A. Ross, K. Lüers, C. Cieslar, R. Rudolph, and T. A. Holak, Structure and dynamics of the human granulocyte colony-stimulating factor determined by NMR spectroscopy. Loop mobility in a four-helix-bundle protein. *Biochemistry* **33,** 8453–8463 (1994).
18. D. R. Muhandiran, T. Yamazaki, B. D. Sykes, and L. E. Kay, Measurement of $^{2}$H $T_1$ and $T_{1\rho}$ relaxation times in uniformly $^{13}$C-labeled and fractionally $^{2}$H-labeled proteins in solution. *J. Am. Chem. Soc.* **117,** 11536–11544 (1995).
19. D. Fushman, S. Cahill, and D. Cowburn, The main-chain dynamics of the dynamin pleckstrin homology (PH) domain in solution: Analysis of $^{15}$N relaxation with monomer/dimer equilibrium. *J. Mol. Biol.* **266,** 173–194 (1997).
20. J. W. Peng and G. Wagner, Mapping of spectral density functions using heteronuclear NMR relaxation measurements. *J. Magn. Reson.* **98,** 308–332 (1992).
21. J. W. Peng and G. Wagner, Mapping of the spectral densities of N–H bond motions in Eglin c using heteronuclear relaxation experiments. *Biochemistry* **31,** 8571–8586 (1992).
22. N. A. Farrow, O. Zhang, A. Szabo, D. A. Torchia, and L. E. Kay, Spectral density function mapping using $^{15}$N relaxation data exclusively. *J. Biomol. NMR* **6,** 153–162 (1995).
23. R. Ishima and K. Nagayama, Protein backbone dynamics revealed by quasi spectral density function analysis of amide N-15 nuclei. *Biochemistry* **34,** 3162–3171 (1995).
24. J.-F. Lefèvre, K. T. Dayie, J. W. Peng, and G. Wagner, Internal mobility in the partially folded DNA binding and dimerization domains of GAL4: NMR analysis of the N–H spectral density functions. *Biochemistry* **35,** 2674–2686 (1996).
25. A. A. Markus, K. T. Dayie, P. Matsudaira, and G. Wagner, Local mobility within Villin 14T via heteronuclear relaxation measurements and a reduced spectral density mapping. *Biochemistry* **35,** 1722–1732 (1996).
26. C. H. M. Papavoine, M. L. Remerowski, L. M. Horstink, R. N. H. Kronings, C. W. Hilbers, and F. J. M. van der Ven, Backbone dynamics of the major coat protein of bacteriophage M13 in detergent micelles by $^{15}$N nuclear magnetic resonance relaxation measurements using the model-free approach and reduced spectral density mapping. *Biochemistry* **36,** 4015–4026 (1997).
27. C. Renner, R. Baumgartner, A. A. Noegel, and T. A. Holak, Backbone dynamics of the CDK inhibitor p19$^{INK4d}$ studied by NMR $^{15}$N relaxation experiments at two field strength. *J. Mol. Biol.* **283,** 221–229 (1998).
28. D. Fushman, N. Tjandra, and D. Cowburn, An approach to direct determination of protein dynamics from $^{15}$N NMR relaxation at multiple fields, independent of variable $^{15}$N chemical shift anisotropy and chemical exchange contributions. *J. Am. Chem. Soc.* **121,** 8577–8582 (1999).
29. M. Zweckstetter and T. A. Holak, An adiabatic multiple spin-echo pulse sequence: Removal of systematic errors due to pulse imperfections and off-resonance properties. *J. Magn. Reson.* **133,** 134–147 (1998).
30. A. Abragam, "Principles of Nuclear Magnetism," Clarendon, Oxford, 1961.
31. V. Y. Orekhov, K. V. Pervushin, D. M. Korzhnev, and A. S. Arsieniev, Backbone dynamics of (1–71)- and (1–36)-bactrioopsin studied by two-dimensional $^{1}$H–$^{15}$N NMR spectroscopy. *J. Biomol. NMR* **6,** 113–122 (1995).
32. D. M. LeMaster, NMR relaxation order parameter analysis of the dynamics of protein side chains. *J. Am. Chem. Soc.* **121,** 1726–1742 (1999).
33. G. Barbato, M. Ikura, L. E. Kay, R. W. Pastor, and A. Bax, Backbone dynamics of calmodulin studied by $^{15}$N relaxation using inverse detected two-dimensional NMR spectroscopy: The central helix is flexible. *Biochemistry* **31,** 5269–5278 (1992).